Quantum Criticality in Monolayer Amorphous Carbon

Rejaul SK,[1] Hanning Zhang,[2] Artem K. Grebenko,[3] Arsen Herasymchuk,[4] Ranjith Shivajirao,[1] Hongji Zhang,[5] Abee Nelson,[1] Zheng Jue Tong,[1] Gagandeep Singh,[1] Naoto Kimiuchi,[6] Yuta Sato,[7] Kazutomo Suenaga,[6] Chee Tat Toh,[5] Rudolf A. Römer,[8] Shaffique Adam,[5,9] Oleg V. Yazyev,[2] Barbaros Özyilmaz†,[3,5] and Bent Weber[1,*]

[1]*Division of Physics and Applied Physics, School of Physical and Mathematical Sciences, Nanyang Technological University, Singapore 637371, Singapore*
[2]*Institute of PhysicsEcole, Polytechnique Fédérale de Lausanne (EPFL), Lausanne CH-1015, Switzerland*
[3]*Department of Physics, National University of Singapore, Singapore 117551, Singapore*
[4]*Department of Physics, University of Zürich, CH-8057 Zürich, Switzerland*
[5]*Department of Materials Science and Engineering, National University of Singapore, Singapore*
[6]*Sanken, Osaka University, Ibaraki, Japan*
[7]*Nanomaterials Research Institute, National Institute of Advanced Industrial Science and Technology (AIST), Tsukuba, Japan*
[8]*Department of Physics, University of Warwick, Gibbet Hill Road, Coventry, CV4 7AL, UK*
[9]*Department of Physics, Washington University in St. Louis, St. Louis, Missouri 63130, USA*

(Dated: June 8, 2026)

SUPPLEMENTARY NOTE ON EXPERIMENT

A. Supplymentary note I: Box-counting method for Multifractal Analysis of LDOS Maps

Multifractal analysis was performed on real-space differential conductance ($\mathrm{d}I/\mathrm{d}V$) maps, which are proportional to the local density of states (LDOS). The LDOS intensity was treated as a normalized spatial probability distribution following the standard multifractal box-counting method [1]. For each conductance map of size L, the image was divided into non-overlapping square boxes of linear size l. The probability measure in box k was defined as

$$P_k(l) = \frac{\sum_{(x,y)\in k} \rho(x,y)}{\sum_{x,y} \rho(x,y)}. \tag{1}$$

such that $\sum_k P_k(l) = 1$. Where $\rho(x,y) = \mathrm{d}I/\mathrm{d}V(x,y)$. To probe the scaling properties of the spatial distribution, the q-dependent normalized measure was constructed [1] as,

$$\mu_k(q,l) = \frac{P_k(l)^q}{\sum_j P_j(l)^q}. \tag{2}$$

Within the Chhabra–Jensen formalism [1], the singularity strength $\alpha(q)$ and fractal spectrum $f(q)$ were obtained directly from the weighted logarithmic averages

$$\alpha(q) = \frac{\sum_k \mu_k(q,l) \ln P_k(l)}{\ln L}, \tag{3}$$

$$f(q) = \frac{\sum_k \mu_k(q,l) \ln \mu_k(q,l)}{\ln L}. \tag{4}$$

The multifractal singularity spectrum $f(\alpha)$ was then obtained parametrically from the dependence of $f(q)$ on $\alpha(q)$. The associated mass exponent (τ_q) and anomalous multifractal exponent (Δ_q) was computed as

$$\tau_q = q\,\alpha(q) - f(q). \tag{5}$$

* Corresponding authors: †barbaros@nus.edu.sg, and *b.weber@ntu.edu.sg

$$\tau_q = d(q-1) + \Delta_q, \tag{6}$$

The analysis was performed over a wide symmetric range of moment orders q spanning both negative and positive values in order to capture the scaling contributions of low- and high-intensity LDOS regions. This procedure enables direct identification of spatially extended, localized, or critical electronic states through the width and shape of the multifractal singularity spectrum $f(\alpha)$. Finally, the generalized fractal dimension (D_q) [2] has been calculated using

$$\tau_q = D_q(q-1), \tag{7}$$

1. *Extraction of multifractality strength γ from the singularity spectrum*

Multifractal wavefunctions near an Anderson critical point exhibit a characteristic singularity spectrum $f(\alpha)$ that characterizes the fractal distribution of amplitudes in disordered electronic wavefunctions by relating the scaling exponent α of local probability densities. In the regime of weak multifractality, analytical treatments based on the nonlinear σ-model [2] predict that the singularity spectrum assumes a parabolic form in the vicinity of its maximum. This provides a convenient way to quantify the strength of multifractal fluctuations through a single parameter(γ).

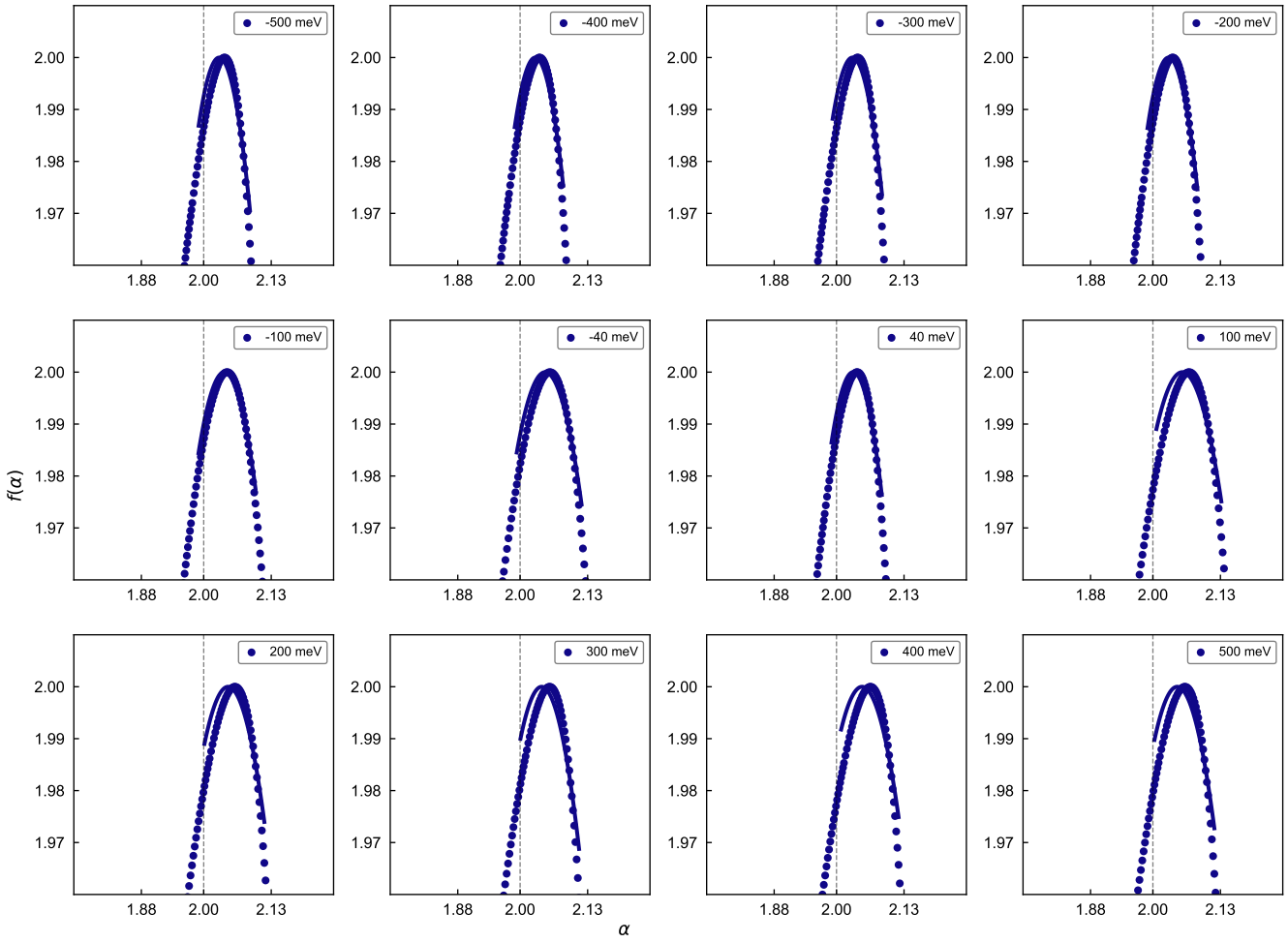

FIG. S1. **Estimation of the multifractality strength γ from the singularity spectrum.** Experimental singularity spectra $f(\alpha)$ for various energy obtained from the multifractal analysis of LDOS maps were fitted using the parabolic eq [34]. Solid curves represent the best fits to the experimental data.

In general spatial dimension d, the parabolic approximation of the singularity [2] spectrum can be written as

$$f(\alpha) = d - \frac{(\alpha - d - \gamma)^2}{4\gamma}, \tag{8}$$

where γ characterizes the strength of multifractal fluctuations and controls the width of the spectrum. The spectrum reaches its maximum value $f(\alpha) = d$ at

$$\alpha_0 = d + \gamma, \tag{9}$$

which corresponds to the most probable scaling exponent of the wavefunction amplitude.
For the present system, which is two-dimensional ($d = 2$), the expression reduces to

$$f(\alpha) = 2 - \frac{(\alpha - 2 - \gamma)^2}{4\gamma}. \tag{10}$$

The experimentally obtained $f(\alpha)$ values were fitted with the above expression using nonlinear least-squares regression, as shown in Fig. S1, treating γ as the only free parameter while fixing the spatial dimensionality to $d = 2$. To ensure the validity of the parabolic approximation, the fitting was restricted to the central region of the spectrum around its maximum. The resulting parameter γ provides a quantitative measure of the width of the singularity spectrum and therefore of the strength of multifractality in the electronic states. The multifractal strength γ extracted from parabolic fitting of the singularity spectrum (Fig. S1). At -40 meV, where $\xi(E)$ diverges, we find $\gamma \approx 0.05$ closely matching that numerically obtained ($\gamma \approx 0.07$) for the Gaussian broadened LDOS maps of MAC.

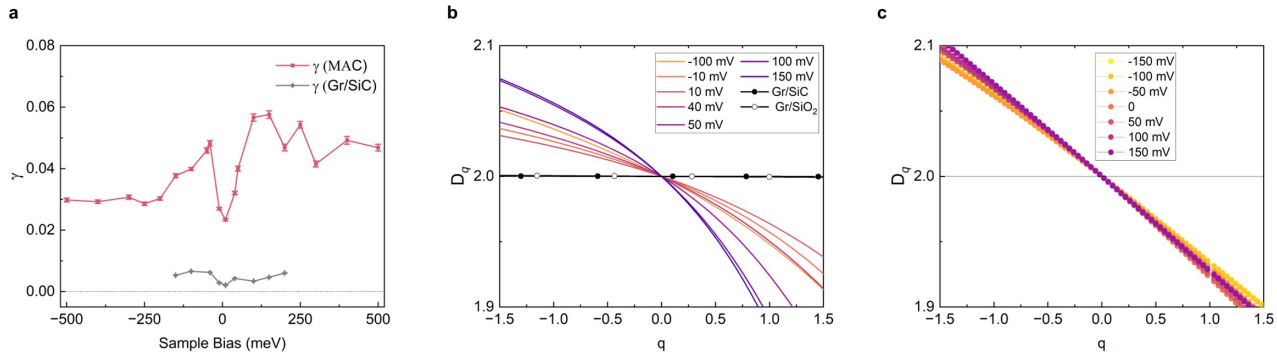

FIG. S2. **Multifractality strength γ and generalized fractal dimensionD_q. a,** Extracted parameter γ characterizes the strength of multifractality. Increased γ values correspond to broader singularity spectra and stronger multifractal fluctuations. **b,** Experimentally extracted generalized fractal dimensions D_q (using eq[27]) plotted as a function of q for graphene and MAC. Graphene exhibits $D_q \approx d = 2$ for all q (where $d = 2$ represent the system dimension, consistent with spatially uniform LDOS fluctuations, indicating extended electronic states. In contrast, MAC shows a non-trivial dependence of D_q on q [2], indicating strong multifractality and spatially inhomogeneous electronic structure, consistent with critical-like electronic states. (c) Numerically calculated D_q for MAC, showing excellent agreement with experimental.

2. *Experimental extraction of anomalous multifractal exponent (Δ_2)*

Within the multifractal framework, the generalized moments obey the scaling relation [2–4]

$$P_q(l) \sim \lambda^{\tau(q)}. \tag{11}$$

where $\lambda = l/L$. For the second moment $q = 2$, this becomes

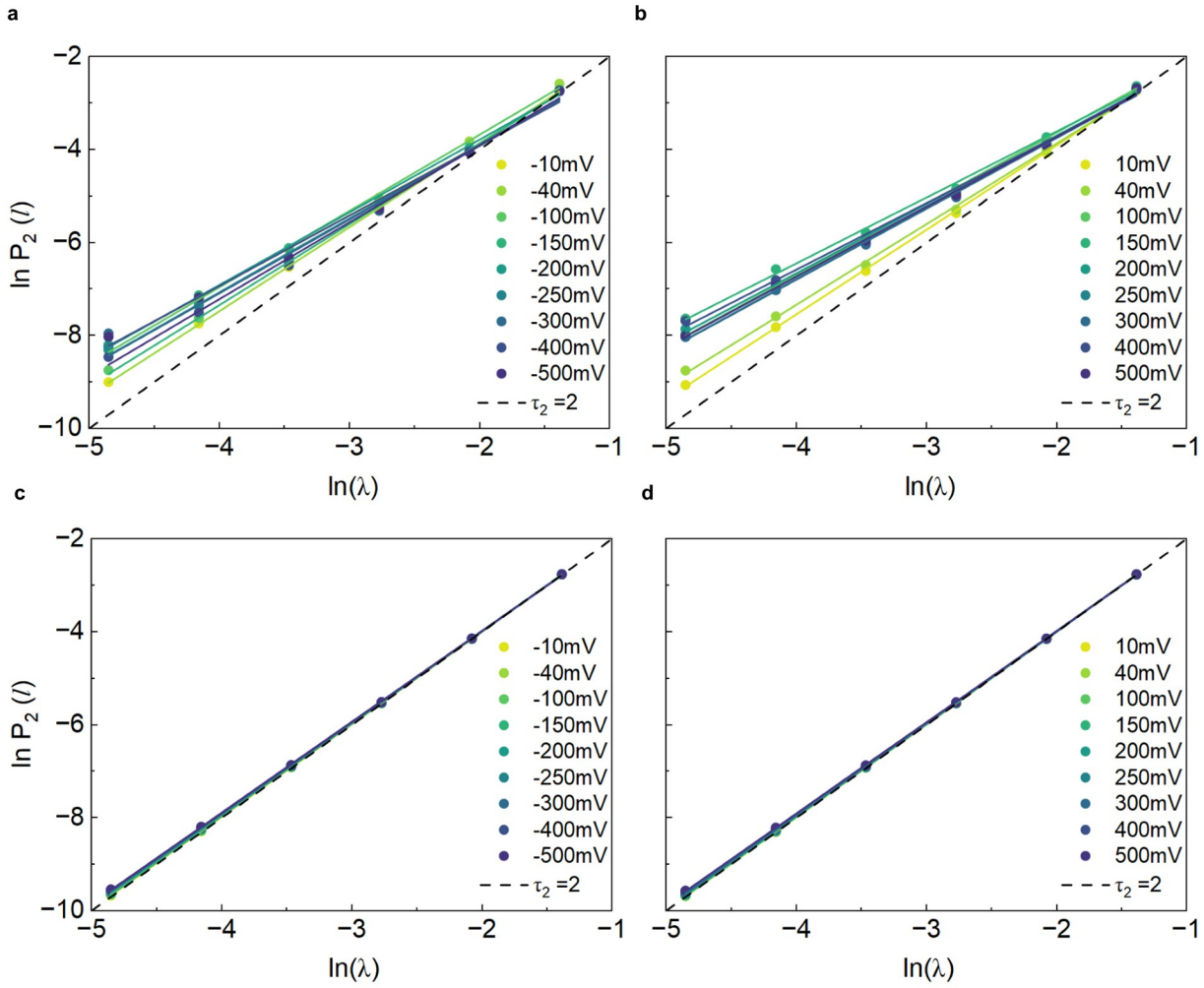

FIG. S3. **Extraction of the multifractal exponent τ_2 from box-counting analysis. a,b,** Log– log plots of the generalized inverse participation ratio $P_2(\ell)$ as a function of box size ℓ for MAC LDOS maps acquired at positive and negative sample biases, respectively. τ_2 estimated from the linear fits (solid lines). **c,d,** Corresponding analysis for graphene LDOS maps at positive and negative sample biases, respectively.

$$P_2(l) \sim \lambda^{\tau_2}. \tag{12}$$

The exponent τ_2 was therefore extracted from the slope of the linear fit in a log–log plot of $P_2(L)$ as a function of box size L,

$$\log P_2(l) = \tau_2 \log \lambda + \text{const.} \tag{13}$$

Linear regression over multiple box sizes was used to determine τ_2. The extracted exponent characterizes the spatial correlations of the LDOS fluctuations [2]. For a metallic two-dimensional system,

$$\tau(2) = 2. \tag{14}$$

Deviations from this value define the anomalous multifractal exponent (Δ_2) [2, 5] which has been estimated using equation [6] for $q = 2$ as below

$$\Delta_2 = \tau(2) - 2, \tag{15}$$

Δ_2 estimated using equation [15] is used in the main text Fig. 3b. The same procedure was applied to the numerically calculated LDOS of MAC as shown in Fig. S5 and obtained Δ_2 results shown in Fig. 3e in main text.

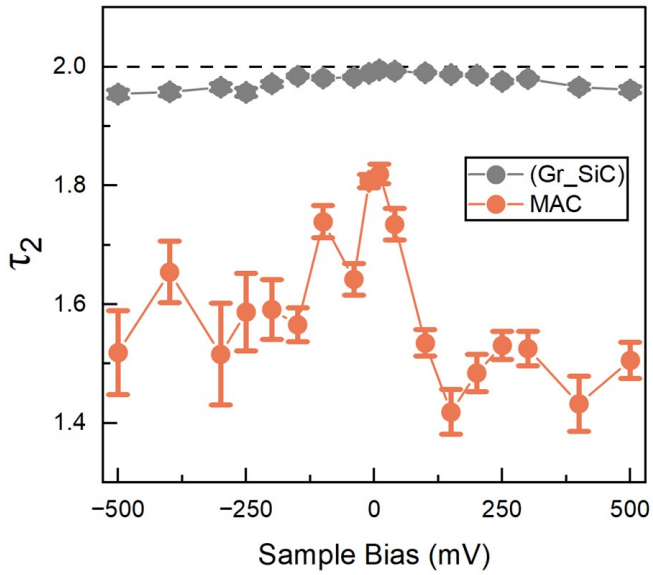

FIG. S4. **Energy-dependent multifractal exponent τ_2.** Extracted τ_2 values for MAC and graphene. While graphene remains close to the system dimension $\tau_2 = d = 2$, MAC exhibits clear deviations from 2, indicating anomalous scaling and critical-like electronic states.

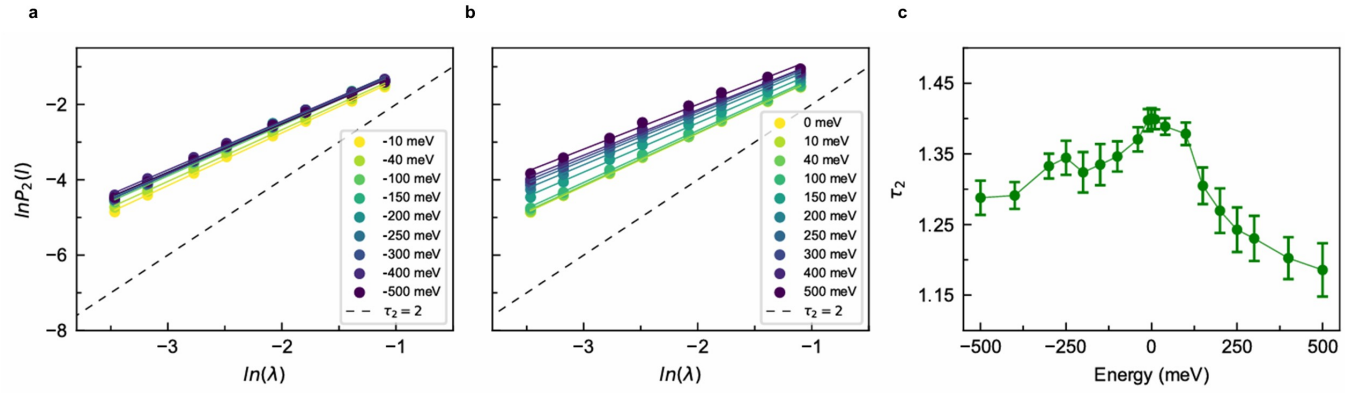

FIG. S5. **Extraction of the multifractal exponent τ_2 using numerically calculated single state LDOS. a,b,** Log–log plots of the generalized inverse participation ratio $P_2(\ell)$ as a function of box size ℓ for numerically calculated LDOS maps of MAC acquired at positive and negative sample biases, respectively. τ_2 estimated from the linear fits (solid lines). **c,** Extracted τ_2 from the fits in (**a,b,**).

B. Supplementary Note II: Two-Dimensional Autocorrelation Analysis of STM/STS Maps

All $\mathrm{d}I/\mathrm{d}V$ maps $g(x, y, E)$ were pre-processed prior to spatial correlation analysis. To isolate spatial fluctuations associated with electronic inhomogeneity, the spatial mean value was subtracted:

$$\delta g(x, y, E) = g(x, y, E) - \langle g(E) \rangle, \tag{16}$$

where $\langle g(E) \rangle$ denotes the spatial average of the conductance map. This procedure removes the uniform background contribution and ensures that correlation analysis probes only spatial fluctuations of the LDOS.

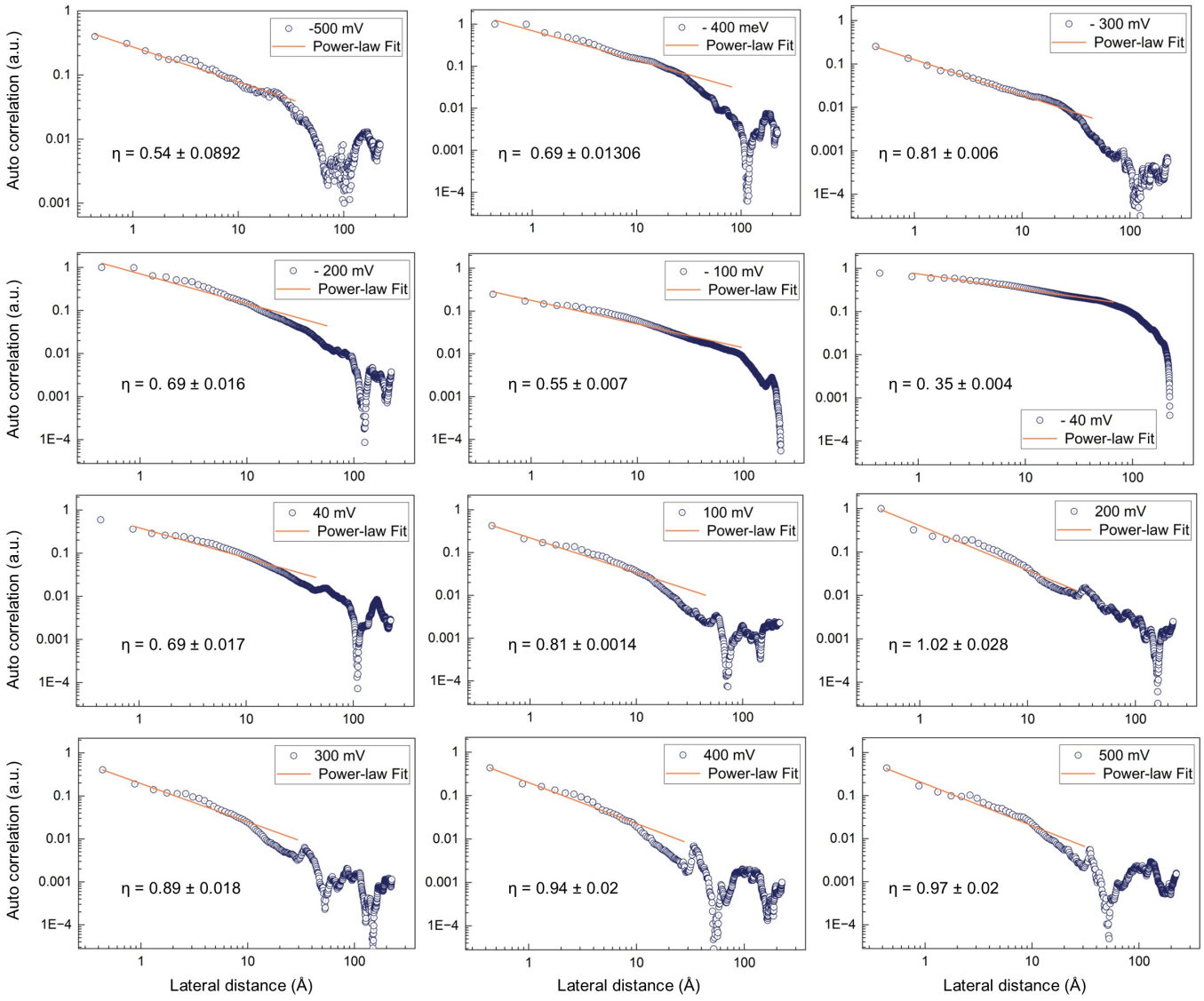

FIG. S6. **Extraction of the correlation-length decay exponent at various energies.** Radially averaged spatial correlation functions $C(r)$ obtained from LDOS maps using Eq [17] at different energies were fitted using a power-law decay function [21]. The fitting range was limited to the well-defined correlation profile and terminated at the noise-dominated decay.

The two-dimensional autocorrelation function (2D-ACF) of the fluctuation map $\delta g(x, y, E)$ was computed in discrete form as

$$C(\tau_x, \tau_y) = \frac{1}{N} \sum_{x,y} \delta g(x, y, E)\, \delta g(x + \tau_x, y + \tau_y, E), \tag{17}$$

where $\tau_x = m\Delta x$ and $\tau_y = n\Delta y$, with Δx and Δy being the spatial pixel sizes and $m, n \in \mathbb{Z}$ denoting integer shift indices. N represents the number of overlapping pixels contributing to each displacement (τ_x, τ_y).

To extract an isotropic measure of spatial correlations, the two-dimensional autocorrelation function was converted into a radially averaged form:

$$C(r) = \langle C(\tau_x, \tau_y) \rangle_{|\tau|=r}, \tag{18}$$

where

$$r = \sqrt{\tau_x^2 + \tau_y^2}. \tag{19}$$

The radial averaging was performed by binning all ACF values within concentric angular width Δr.

The spatial correlation length ξ was extracted from the decay of the radially averaged autocorrelation function $C(r)$. In disordered electronic systems, the decay is typically well described by an exponential form:

$$C(r) \propto \exp(-r/\xi). \tag{20}$$

For datasets exhibiting critical electronic behavior, deviations from exponential decay were observed in the radial autocorrelation function. In such cases, the long-range behavior was found to follow a power-law form:

$$C(r) \propto r^{-\eta}, \tag{21}$$

where η is the critical exponent characterizing the spatial decay of electronic correlations. The correlation length ξ was obtained by fitting of $C(r)$ within the regime where the correlation decays from its maximum to $1/e$. The experimentally and numerically extracted values of η are shown in Fig. 3b and 3e, respectively.

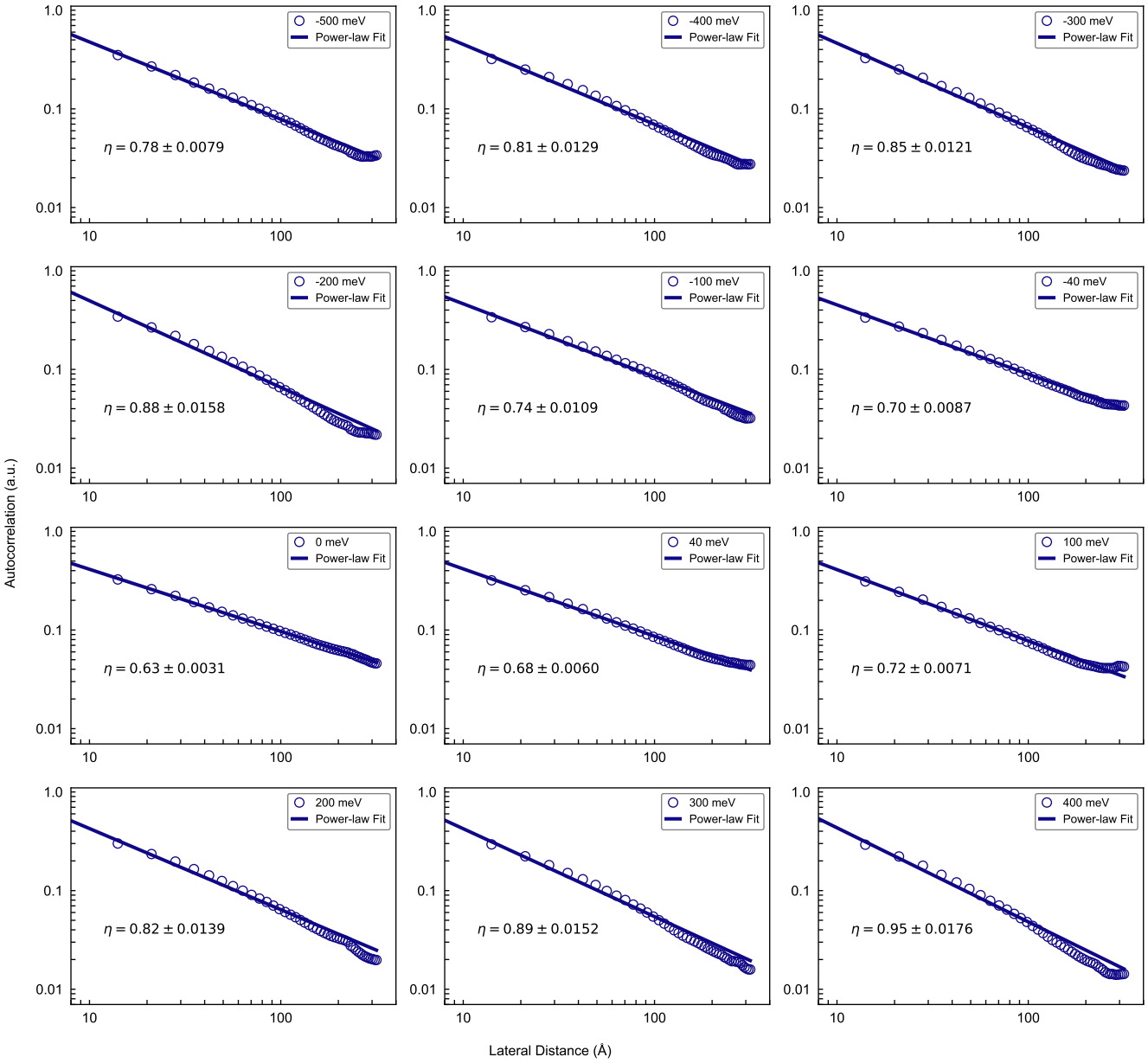

FIG. S7. **Extraction of the correlation-length spatial decay from numerically calculated single state LDOS.** Radially averaged spatial correlation functions $C(r)$ obtained from numerically calculated LDOS maps using Eq (17) at different energies were fitted using a power-law decay function Eq (21).

SUPPLEMENTARY NOTE ON THEORY

C. Supplementary Note III: Low-energy model of graphene with N defects

The graphene sheet with topological defects and strains in the low-energy limit can be modeled using the Dirac equation on curved spacetime [6, 7]. Each localized at the point $\mathbf{x}$ topological defect (pentagon or heptagon disinclination) induces locally nonzero curvature on a graphene sheet, which is given by:

$$R = \frac{2\pi\beta}{3}\delta(\mathbf{x}), \tag{22}$$

where $\beta \in \{-1, 0, 1\}$ correspond to the excess angle from the heptagon defect (-1), no defect (0), and the deficit angle from the pentagon defect $(+1)$. Thus, by introducing the topological defects at the points $\{\mathbf{x}_k\}_{k=1}^N$ and assigning a corresponding β_k to each defect, the resulting metric $g_{\mu\nu}$ is defined as follows:

$$ds^2 = -dt^2 + e^{-2\sigma(\mathbf{x})}\left(dx_1^2 + dx_2^2\right), \tag{23}$$

where $\sigma(\mathbf{x}) = \sum_{k=1}^N \frac{\beta_k}{6} \log|\mathbf{x} - \mathbf{x}_k|$ [8]. Explicitly, the Dirac equation on such manifold with the metric (23) is given by [8, 9]:

$$\left\{ i\gamma^0\partial_t + i\gamma^1 e^{\sigma(\mathbf{x})}\left[\partial_{x_1} - \frac{1}{2}\sigma_{12}\partial_{x_2}\sigma(\mathbf{x})\right] + i\gamma^2 e^{\sigma(\mathbf{x})}\left[\partial_{x_2} + \frac{1}{2}\sigma_{12}\partial_{x_1}\sigma(\mathbf{x})\right]\right\}\psi = 0. \tag{24}$$

Here, we use the following convention for the wave function $\psi = (\psi_{A+}, \psi_{B+}, \psi_{B-}, \psi_{A-})^T$, thus the gamma matrices are given by $\gamma_{1,2} = \tau_3 \otimes \sigma_{1,2}$, where σ_i and τ_i are the Pauli matrices in the $A-B$ and valley subspaces. Thus, we obtain the corresponding Hamiltonian of the system:

$$\mathcal{H}(\omega, \mathbf{x}) = \omega - i\gamma^0\gamma^1 e^{\sigma(\mathbf{x})}\left[\partial_{x_1} - \frac{1}{2}\sigma_{12}\partial_{x_2}\sigma(\mathbf{x})\right] - i\gamma^0\gamma^2 e^{\sigma(\mathbf{x})}\left[\partial_{x_2} + \frac{1}{2}\sigma_{12}\partial_{x_1}\sigma(\mathbf{x})\right]. \tag{25}$$

Notice that the Hamiltonian $\mathcal{H}$ commutes with the matrices:

$$T^1 = \frac{1}{2}\gamma^5 = \frac{1}{2}\tau_3 \otimes \sigma_0, \quad T^2 = \frac{i}{2}\gamma^3 = \frac{1}{2}\tau_2 \otimes \sigma_3, \quad T^3 = \frac{1}{2}\gamma^3\gamma^5 = \frac{1}{2}\tau_1 \otimes \sigma_3, \tag{26}$$

which construct the $SU(2)$ symmetry group built with these generators.

More importantly to the induced curvature by the defects, the boundary condition for the wave function is modified by the defects. After going around a closed path around a single defect we obtain [7]:

$$\begin{aligned} &\psi(r, \phi + 2\pi) = R\psi(r, \phi), \ R \text{ - exchanges } A \leftrightarrow B \text{ and } K \leftrightarrow K', \ R^2 = -I, \\ &\psi(r, \phi + 4\pi) = -\psi(r, \phi). \end{aligned} \tag{27}$$

Therefore, the operator R for a single defect can be chosen as linear combination of T^2 and T^3, thus one may state that after encircling a topological defect, the phase, acquired after the exchange of $K \leftrightarrow K'$ points is arbitrary, and since the operator R_k for the defect at $\mathbf{x}_k$ is defined as follows:

$$R_k = -i\cos(\theta_k)\,\tau_1 \otimes \sigma_3 - i\sin(\theta_k)\,\tau_2 \otimes \sigma_3, \tag{28}$$

where θ_k defines the acquired phase related to the pentagon or heptagon defect, hence related to the deficit angle.

Let us assume that we have a countable amount of defects which are characterized by the set of parameters $\{\mathbf{x}_k, \theta_k\}$. To ensure that the encircling of the defect in the vicinity of $\mathbf{x}_k$ would lead to the change in the wavefunction precisely from that defect, we need to construct the manifold $\mathcal{M}$ in such a way that the corresponding cuts, where the graphene sheet is taped because of the defect, do not intersect. Indeed, for the countable set K of such points, there exist a point P_0, such as for any $P_i, P_j \in K$, $i \neq j$, the rays $R_{i,j}$ with the initial point at P_0 intersect only at P_0, or equivalently, that for any $P_i, P_j \in K$, $i \neq j$, the points P_0, P_i, P_j are not collinear. Indeed, if we define the set of lines $L = \{L_{ij}, i \neq j\}$ passing through points P_i, P_j, then any point $P_0 \in \mathbb{R}^2 \setminus L$ satisfies the condition $R_i \cap R_j = \{P_0\}$, $\forall i \neq j$. Therefore, the holonomy along the closed contours C and $\tilde{C}$, presented in Fig. S8 are the same.

Therefore, the total holonomy is given by the holonomy from the enclosed contour on the flat submanifold and the product of the holonomies from each encircled defect:

$$\psi(r, \phi + 2\pi) = U_C\psi(r, \phi) = U_{\tilde{C}}\psi(r, \phi) = e^{\frac{i}{2}\gamma_1\gamma_2 2\pi}\prod_{k=1}^N R_k\psi(r, \phi). \tag{29}$$

The product can be simplified as follows:

$$\prod_{k=1}^N R_k = (-1)^{N-1}e^{-i\sum_{k=1}^N(-1)^{k-1}\theta_k\tau_3\otimes\sigma_0}\left(\tau_1 \otimes \sigma_3\right)^N. \tag{30}$$

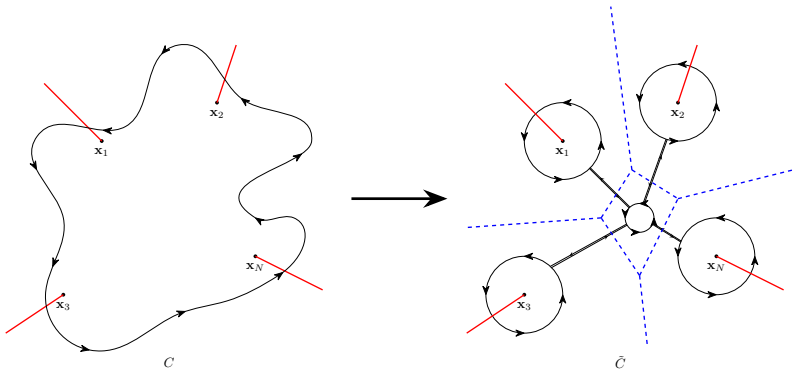

FIG. S8. Contours C and $\tilde{C}$ enclosing N multiple defects

By defining the corresponding gauge field $\mathbf{B}_k$ as:

$$\oint_{C_k} (\mathbf{B}_k \cdot d\mathbf{x}) = (-1)^{k-1} 2\theta_k \;\Rightarrow\; \mathbf{B}_k = \frac{(-1)^{k-1}\theta_k}{\pi} \frac{(x_1 - x_{1,k})\,\mathbf{e}_2 - (x_2 - x_{2,k})\,\mathbf{e}_1}{|\mathbf{x} - \mathbf{x}_k|^2}, \tag{31}$$

we obtain that

$$\psi(r, \phi + 2\pi) = (-1)^N e^{-i\sum_{k=1}^N \oint_{C_k} (\mathbf{B}_k \cdot d\mathbf{x}) \frac{1}{2}\tau_3 \otimes \sigma_0} (\tau_1 \otimes \sigma_3)^N \psi(r, \phi). \tag{32}$$

Therefore, after the gauge transformation of the wave function to restore the BC $\psi'(r, \phi+2\pi) = -\psi'(r, \phi)$ for arbitrary contour C [7], we obtain the following modification of the Hamiltonian:

$$\begin{aligned} \mathcal{H}(\omega, \mathbf{x}) = \omega &- i\gamma^0\gamma^1 e^{\sigma(\mathbf{x})} \left[\partial_{x_1} - \frac{1}{2}\sigma_{12}\partial_{x_2}\sigma(\mathbf{x}) + i\frac{1}{2}\sum_{k=1}^N B_{1,k}(\mathbf{x}) (\tau_1 \otimes \sigma_3)^N (\tau_3 \otimes \sigma_0) (\tau_1 \otimes \sigma_3)^N\right] \\ &- i\gamma^0\gamma^2 e^{\sigma(\mathbf{x})} \left[\partial_{x_2} + \frac{1}{2}\sigma_{12}\partial_{x_1}\sigma(\mathbf{x}) + i\frac{1}{2}\sum_{k=1}^N B_{2,k}(\mathbf{x}) (\tau_1 \otimes \sigma_3)^N (\tau_3 \otimes \sigma_0) (\tau_1 \otimes \sigma_3)^N\right]. \end{aligned} \tag{33}$$

By taking the limit $N \to \infty$ and using the central limit theorem, it can be demonstrated that the resulting effective gauge field $B_\mu(\mathbf{x}) = B_\mu^a(\mathbf{x})T^a$ satisfies the Gaussian distribution

$$P[B_\mu] \propto \exp\left\{-\frac{1}{2\pi g_B}\int d^2x \,\mathrm{tr}\,[B_\mu(\mathbf{x})B_\mu(\mathbf{x})]\right\}, \tag{34}$$

for which, as the size of the system increases, the strength of disorder diverges $g_B \to \infty$ logarithmically with system size [10].

For simplicity, the effects of the modified Fermi velocity by the function $\sigma(\mathbf{x})$ will be neglected, thus we consider the final form of the Hamiltonian

$$\mathcal{H}(\omega, \mathbf{x}) = \omega + \gamma^0\gamma^\mu \left(-i\partial_\mu + A_\mu(\mathbf{x}) + B_\mu^a(\mathbf{x})T^a\right), \;\mu = 1, 2. \tag{35}$$

The $SU(2)$ field B_μ encodes the role of the disclinations (expressed through induced boundary conditions) as discussed above, acquiring the additional terms, written explicitly as:

$$\begin{aligned} &\Delta H_B \propto \gamma^0\gamma^1 T^1 = \tau_0 \otimes \sigma_1, \quad \Delta H_B \propto \gamma^0\gamma^1 T^2 = \tau_1 \otimes \sigma_2, \quad \Delta H_B \propto \gamma^0\gamma^1 T^3 = \tau_2 \otimes \sigma_2, \\ &\Delta H_B \propto \gamma^0\gamma^2 T^1 = \tau_0 \otimes \sigma_2, \quad \Delta H_B \propto \gamma^0\gamma^2 T^2 = \tau_1 \otimes \sigma_1, \quad \Delta H_B \propto \gamma^0\gamma^2 T^3 = \tau_2 \otimes \sigma_1. \end{aligned} \tag{36}$$

The $U(1)$ field A_μ corresponds to the strains induced by the defects and is assumed to follow the probablity distribution:

$$P[A_\mu] \propto \exp\left\{-\frac{1}{4\pi g_A}\int d^2x \, A_\mu(\mathbf{x})A_\mu(\mathbf{x})\right\}. \tag{37}$$

A straightforward calculation shows that chiral symmetry $C_0 : A \to -\tau_0 \otimes \sigma_3 \, A \, \tau_0 \otimes \sigma_3$ is preserved [11], as emphasized in the main text. This symmetry together with the low-energy Hamiltonian (35) corresponds to the WZW criticality at $\omega = 0$.

D. Supplementary Note IV: WZW predictions and comparison to numerical data

For the Hamiltonian (35), the partition function for a given realization of the disorder A_μ and B_μ (which belongs to the $su(N)$ algebra, $N = 2$) reads as follows:

$$Z[A_\mu, B_\mu] = \int \mathcal{D}\psi \mathcal{D}\bar{\psi} \, e^{-\int d^2x \psi^\dagger(\mathbf{x}) \mathcal{H}(\omega, \mathbf{x}) \psi(\mathbf{x})}. \tag{38}$$

Therefore, the impurity average of the correlation function $\mathcal{O}\left[\psi, \bar{\psi}\right]$ is given by:

$$\langle \mathcal{O} \rangle = \int_{U(1)} \mathcal{D}A_\mu \, P[A_\mu] \int_{SU(N)} \mathcal{D}B_\mu \, P[B_\mu] \int \mathcal{D}\psi \mathcal{D}\bar{\psi} \, \mathcal{O}\left[\psi, \bar{\psi}\right] e^{-\int d^2x \psi^\dagger(\mathbf{x}) \mathcal{H}(\omega, \mathbf{x}) \psi(\mathbf{x})}. \tag{39}$$

Following [12–14], the theory becomes conformal at $\omega = 0$ and $g_B \to \infty$, and one can calculate the impurity averaged correlation functions by decomposing the partition function in free fermion (disorder independent) part, the extension $U(1)$ part in which a strain dependence is concentrated, and the complex extension $SU^C(N)$ part in which a disorder dependence is concentrated. The later part gives rise to the Wess-Zumino-Witten topological term [12, 14]. Indeed, by working in the chiral basis for the spinors $\psi = (\psi_+, \psi_-)^T$ and introducing the holomorphic and antiholomorphic derivatives and fields

$$\begin{aligned} \partial_z &= \frac{1}{2}\left(\partial_1 - i\partial_2\right), \quad A_z = \frac{1}{2}\left(A_1 - iA_2\right), \quad B^a_z = \frac{1}{2}\left(B^a_1 - iB^a_2\right) \\ \partial_{\bar{z}} &= \frac{1}{2}\left(\partial_1 + i\partial_2\right), \quad A_{\bar{z}} = \frac{1}{2}\left(A_1 + iA_2\right), \quad B^a_{\bar{z}} = \frac{1}{2}\left(B^a_1 + iB^a_2\right) \end{aligned} \tag{40}$$

one can parametrize the components of the gauge fields by fields in the complex extensions:

$$\begin{aligned} A_z &= i\left(2\partial_z H_z\right) H_z^{-1}, \; H_z = e^{-i\phi_z}, \\ A_{\bar{z}} &= i\left(2\partial_{\bar{z}} H_{\bar{z}}\right) H_{\bar{z}}^{-1}, \; H_{\bar{z}} = e^{-i\phi_{\bar{z}}} \\ B_z &= i\left(2\partial_z G_z\right) G_z^{-1}, \; G_z \in SU^C(N) \\ B_{\bar{z}} &= i\left(2\partial_{\bar{z}} G_{\bar{z}}\right) G_{\bar{z}}^{-1}, \; G_{\bar{z}} \in SU^{C*}(N) \end{aligned} \tag{41}$$

Note, that such change of variables introduces auxiliary Grassmann fields $(\alpha^a_\pm, \beta^a_\pm)$, $a = 0, ..., N$; see Ref. [12] for details. This allows to decouple the vector gauge fields from the field ψ via:

$$\begin{aligned} \psi_+ &= H_{\bar{z}} G_{\bar{z}} \psi'_+, \quad \psi^\dagger_+ = \psi'^\dagger_+ G^{-1}_{\bar{z}} H^{-1}_{\bar{z}} \\ \psi_- &= H_z G_z \psi'_-, \quad \psi^\dagger_- = \psi'^\dagger_- G^{-1}_z H^{-1}_z \end{aligned} \tag{42}$$

The Jacobian of this transformation Therefore, Eq. (39) can be rewritten as follows:

$$\langle \mathcal{O} \rangle = \int \mathcal{D}H_z \mathcal{D}H_{\bar{z}} \int \mathcal{D}G_z \mathcal{D}G_{\bar{z}} \int \prod_{a=0}^{N} \mathcal{D}\alpha^a_\pm \mathcal{D}\beta^a_\pm \int \mathcal{D}\psi' \mathcal{D}\bar{\psi}' \, \mathcal{O}\left[HG\psi', \psi'^\dagger G^{-1} H^{-1}\right] e^{-S_\psi - S_{\text{ghost}} - S_A - S_B} \tag{43}$$

where

$$\begin{aligned} S_\psi &= \int d^2x \left[\psi'^\dagger_+ 2\partial_{\bar{z}} \psi'_+ + \psi'^\dagger_- 2\partial_z \psi'_-\right] \\ S_A &= \frac{1}{2g_A N} \Gamma[G_z G_{\bar{z}}] - \frac{1}{2g_A N} \Gamma[G^\dagger_{\bar{z}} G_{\bar{z}}] \\ S_B &= -2N \, \Gamma[G^\dagger_{\bar{z}} G_{\bar{z}}] \end{aligned} \tag{44}$$

with

$$\Gamma[h] = \frac{1}{8\pi}\int_{\partial B} dx_1 dx_2 \,\mathrm{tr}\left[(\partial_\mu h)\left(\partial_\mu h^{-1}\right)\right] + \frac{i}{12\pi}\int_B dx_1 dx_2 dx_3\, \epsilon_{\mu\nu\lambda}\,\mathrm{tr}\left[(\partial_\mu h)\, h^{-1}\,(\partial_\nu h)\, h^{-1}\,(\partial_\lambda h)\, h^{-1}\right]. \tag{45}$$

Here, S_B is the action for the field $G_{\bar{z}}^{\dagger} G_{\bar{z}}$ with the second term in Eq. (45) being the Wess-Zumino term, defining the WZW functional on level $k = -2N$. Such separation of the partition function into four independent parts allows to calculate the conformal weights. For a detailed and rigorous derivation, see Ref. [12].

Thus, the scaling of the density-density correlation function for $\rho(\omega; x)$ at $\omega = 0$ can be calculated via operator product expansion (OPE) [12]:

$$\rho(0;x)\rho(0;y) \propto |x-y|^{-2(2h_1-h_2)}\,\rho^2(0;y) \propto |x-y|^{-\frac{2(N-1)}{N^2}-4g_A}\,\rho^2(0;y), \tag{46}$$

with $h_q = \frac{q}{2} - g_A q^2 - \frac{N-1}{2N^2}\left(q^2 + Nq\right)$. The critical index is given by $\eta = 4g_A + 2(N-1)/N^2$ with the multifractal exponent $\gamma = 2g_A + (N-1)/N^2$. The density of states scales with energy as:

$$\rho(\omega) \propto \omega^{\frac{1-2g_A N^2}{2(1+g_A)N^2-1}} \;\Rightarrow\; \text{DOS exponent: } \beta = \frac{1-2g_A N^2}{2\,(1+g_A)\,N^2-1} =: \frac{2-z}{z} \;\Longrightarrow\; z = 1 + 2g_A + \frac{N^2-1}{N^2} \tag{47}$$

For $N = 2$ and $g_A = 0$, we obtain $\eta = 1/2$, the multifractal exponent $\gamma = 1/4$, and the density of states exponent $z = 7/4$. By introducing a small value $g_A \approx 0.05$, one obtains a good agreement with the numerical data.

	Theoretical $g_A = 0$	Theoretical $g_A = 0.05$	Numerical
η	1/2	0.7	0.63
γ	1/4	0.35	0.34
z	7/4	1.85	1.848

TABLE I. Comparison of theoretical and numerical values for η, γ, and z. The numerical values are obtained from the correlation function analysis in Fig 3.e and Fig. S7 (η), multifractal analysis Fig. S9 (γ).

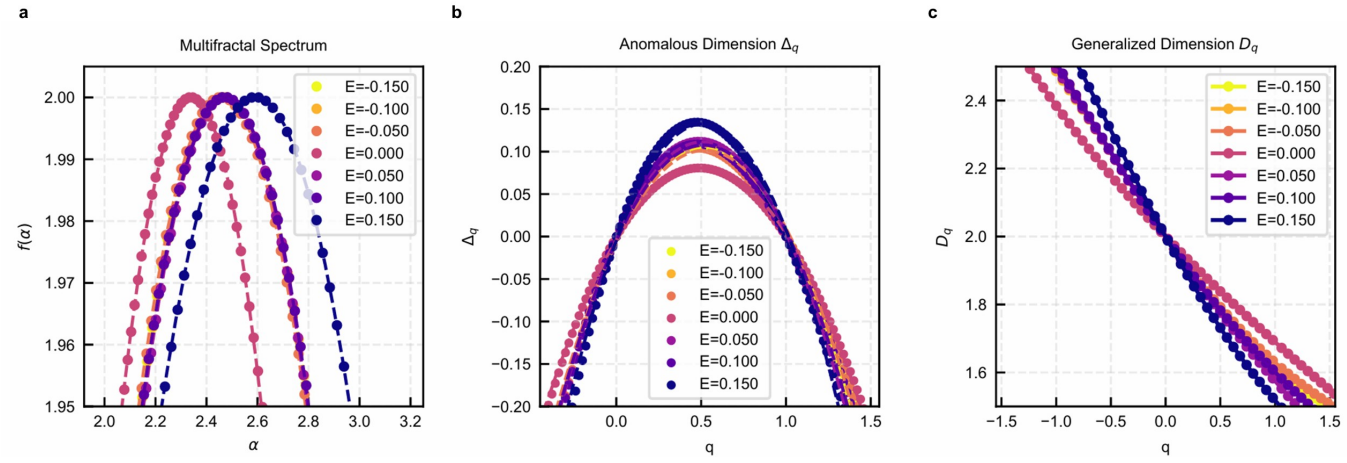

FIG. S9. **Multifractal analysis of a numerically calculated single-state wavefunction. a**, Singularity spectrum $f(\alpha)$ (points), with a parabolic fit shown as dotted lines, yielding γ=0.34 at E=0. **b**, Anomalous multifractal exponent Δ_q as a function of moment order q. **c**, Generalized fractal dimension D_q, revealing the nontrivial scaling behaviour of the electronic state. Broader $f(\alpha)$, nonlinear dependence of Δ_q and D_q on q confirms the multifractal nature of the electronic state. In contrast to the LDOS maps shown in Fig. 2j and Fig.2l, the LDOS maps here correspond to single-state data without additional energy broadening.

[1] A. Chhabra and R. V. Jensen, Direct determination of the $f(\alpha)$ singularity spectrum, Physical Review Letters **62**, 1327 (1989).
[2] F. Evers and A. D. Mirlin, Anderson transitions, Reviews of Modern Physics **80**, 1355 (2008).
[3] M. Janssen, Multifractal analysis of broadly-distributed observables at criticality, International Journal of Modern Physics B **8**, 943 (1994).
[4] A. Rodriguez, L. J. Vasquez, and R. A. Römer, Multifractal analysis of the metal-insulator transition in the three-dimensional Anderson model. ii. symmetry relation under ensemble averaging, Physical Review B—Condensed Matter and Materials Physics **78**, 195107 (2008).
[5] A. Rodriguez, L. J. Vasquez, K. Slevin, and R. A. Römer, Multifractal finite-size scaling and universality at the Anderson transition, Physical Review B **84**, 134209 (2011).
[6] M. Vozmediano, M. Katsnelson, and F. Guinea, Gauge fields in graphene, Physics Reports **496**, 109 (2010).
[7] Y. Sitenko and N. Vlasii, Electronic properties of graphene with a topological defect, Nuclear Physics B **787**, 241 (2007).
[8] A. Cortijo and M. A. H. Vozmediano, Electronic properties of curved graphene sheets, Europhysics Letters **77**, 47002 (2007).
[9] A. Vilenkin and E. P. S. Shellard, *Cosmic Strings and Other Topological Defects* (Cambridge University Press, 2000).
[10] J. González, F. Guinea, and M. A. H. Vozmediano, Electron-electron interactions in graphene sheets, Phys. Rev. B **63**, 134421 (2001).
[11] F. Evers and A. D. Mirlin, Anderson transitions, Rev. Mod. Phys. **80**, 1355 (2008).
[12] C. Mudry, C. Chamon, and X.-G. Wen, Two-dimensional conformal field theory for disordered systems at criticality, Nuclear Physics B **466**, 383 (1996).
[13] A. Nersesyan, A. Tsvelik, and F. Wenger, Disorder effects in two-dimensional Fermi systems with conical spectrum: exact results for the density of states, Nuclear Physics B **438**, 561 (1995).
[14] J.-S. Caux, N. Taniguchi, and A. Tsvelik, Disordered Dirac fermions: Multifractality termination and logarithmic conformal field theories, Nuclear Physics B **525**, 671 (1998).